Research Square

Preprints are preliminary reports that have not undergone peer review.
They should not be considered conclusive, used to inform clinical practice,
or referenced by the media as validated information.

# Patches of Dual Functions for Wideband MIMO Array Antenna with Linear or Circular Polarization Characteristics

**Reza Zaker**
Azarbaijan Shahid Madani University
**Mohsen Khalily** ( m.khalily@surrey.ac.uk )
University of Surrey, ICS
**Rahim Tafazolli**
University of Surrey, ICS
**Ahmed A. Kishk**
Concordia University

**Research Article**

**Keywords:** MIMO array antenna, novel technique, subminiature structure, linearly-polarized array

**Posted Date:** September 20th, 2021

**DOI:** https://doi.org/10.21203/rs.3.rs-883060/v1

**License:** This work is licensed under a Creative Commons Attribution 4.0 International License.
Read Full License

# Patches of Dual Functions for Wideband MIMO Array Antenna with Linear or Circular Polarization Characteristics

**Reza Zaker[1], Mohsen Khalily[2], Rahim Tafazolli[2], and Ahmed A.Kishk[3]**

[1]Department of Electrical Engineering; Azarbaijan Shahid Madani University, Tabriz, Iran
[2]Institute for Communication Systems (ICS), 5G and 6G innovation centers (5GIC & 6GIC), University of Surrey, Guildford, GU2 7XH, UK
[3]Department of Electrical and Computer Engineering, Concordia University, Montreal, Canada
*Corresponding author email: m.khalily@surrey.ac.uk

## ABSTRACT

In this paper, a design of a monopole-based four-element MIMO array antenna is proposed. The design is based on a novel technique that makes a patch be a ground plane of the next patch. Thus, each patch has a dual function. This method is named the sharing technique. Thus, for the first time, two of such antennas can be merged, providing a subminiature structure. The method is introduced step by step. Then, a 2×2 MIMO array with a total area of 49×49 mm$^2$ is designed, which provides a miniaturized of 57% (from 0.18$\lambda_0^2$ to 0.076$\lambda_0^2$ @ 1.7GHz). Two linearly-polarized array samples are evaluated. One sample with center-fed patches and another with off-center-fed. Both samples provide a semi-end-fire pattern with a minimum front-to-back (F/B) ratio of 11dB and 360° rotation capability with wide 10-dB $S_{11}$ bandwidths over 100%. Moreover, an ultra-wideband circularly polarized array with broadside radiation can be achieved by simultaneous, sequential exciting all ports. The antenna achieves isolation better than 15dB, peak efficiency of 95%, and 5.9dBi gain verified with different measurements.

## Introduction

MULTI-INPUT multi-output (MIMO) technologies play a key role in different wireless communication systems, 4G, 5G, and beyond 5G (B5G) to improve the spectrum, energy efficiencies, and aggregate capacity in a limited frequency spectrum[1–5]. The present and future MIMO structures have to employ an unprecedented number of antennas in an integrated compact volume. The size limitation and great proximity of the antenna elements result in high spatial correlation and mutual coupling between the antennas[5,6]. Therefore, the signal-to-noise ratio and radiation efficiency of large scale antenna arrays, the convergence of array signal processing algorithms, channel capacity, and diversity parameters of any MIMO system are severely degraded[6–9]. Therefore, the expected Quality of Service (QoS) for new networks will be significantly deteriorated. The impedance bandwidth may improve by coupling between antennas. As a final result, introducing an array design applicable for different MIMO systems with an increased number of antennas in limited size and also with standard MIMO performance metrics is an important issue. Hence, in recent years, it has become a focused area of study.

Different decoupling techniques were applied to two-port schemes[6,7,9–18], which can be divided into different categories, including:

**Decoupling Circuit Networks** These efficient networks[6,10–12] are defined by introducing the desired matching and decoupling Z/Y/ABCD/Scattering matrixes between two ports for symmetric or asymmetric arrays to provide the preferred isolation and matching, simultaneously. These designs of narrow-band (less than 20%) have a complicated and vast feeding network.

**Characteristic Modes Theory (CMT)** Based on this theory[13,14], first, the E-field and current distributions on the ground plane of the mobile terminals are illustrated and studied, and then, the antennas are located in the positions with null fields or maximum differences to provide high isolation. The CMT-based MIMO antennas present relatively high efficiency and excellent diversity performance while their matching is mostly moderate.

**Artificial Isolating Structures** These designs such as Defected Ground Structures (DGSs), Electro-magnetic Band Gap (EBG), and metamaterials[7,9,15–18] obtain a band-rejection behavior at a specific frequency band related to the antenna bandwidth. These decoupling structures mostly need a large area between the antennas. Besides, some of them have multiple layers with via which complicate the implementation. Moreover, the back-side radiation in DGSs can degrade the front-to-back (F/B) ratio and the total gain[15]. Another type of these structures is the Frequency Selective Surfaces (FSS), which can change the

polarization of the coupled radiation between two antennas to improve the isolation[17].

In contrast to the two-port MIMO antennas, four-element MIMO designs were introduced in a 2×2 arrangement to provide better spatial diversity and higher total gain[19]. Narrow-dual-band performance and large size are the drawbacks of this antenna. In[20], a four-element structure of compact size of $0.33\lambda_0 \times 0.33\lambda_0$ @ 2.48GHz consists of a pair of printed F-antennas on the top layer, and a pair of a quarter wavelength slot antennas in the back layer achieved about 7% of 10-dB $S_{11}$ bandwidth and isolation better than 8dB. In[20], high isolation of 35dB, a gain of 6.8dBi, and an envelope correlation coefficient (ECC) less than 0.05 were provided for a tightly spaced four-element ($1.2\lambda_0 \times 1.2\ \lambda_0$), the thickness of 14mm with a three-layer multi-via MIMO antenna employing five discrete mushroom-like EBG structures. A very narrow bandwidth (less than 2%) around 2.45GHz was achieved. To overcome these disadvantages and enhance the system characteristics, four-element 2×2 MIMO designs were presented in[22–27]. In[22] and[23], the smallest area (less than $0.12\lambda_0^2$), efficiency of 90%, and isolation better than 14dB were achieved. In[27], the widest impedance bandwidth (over 126%) with minimum isolation of about 16dB was presented. In addition,[23] and[26] had used different slots in the ground plane to provide a higher peak gain (over 6.3dB), and very low ECC (less than 0.02). Good diversity and MIMO performances, including efficiency over 95%, ECC less than 0.1, and mean effective gain (MEG) ratio close to 1,were obtained in[24] by using four simple L-shaped monopoles with an interconnected ground plane. However, its isolation level is about 11dB.

In the last decade, few of multi-port MIMO antennas have been proposed with end-fire radiation and circular polarization (CP) characteristics[28–32]. In[29], not Yagi-Uda design with four MIMO antenna units rotated around a circle was non-planar; thus, it is unsuitable for printed circuit (PCB) technology. On the other hand,[28] and[30] presented three-port Yagi-Uda-based structures in PCB technology with high isolation and efficiency, but with less than 5% bandwidth around 5.5GHz with multiple directional beams. These have proven that high spatial un-correlation and capacity can be provided in a rich multipath environment by carefully adjusting the position and size of the parasitic elements. In[31], the MIMO antenna has shown that a fractal Amer-shaped slot radiation element with four ports can be used to obtain unique narrowband CP characteristics for each exciting port.

In this paper, a novel technique is used to have easy-to-fabricate four-port square monopole antennas to achieve an integrated compact MIMO design with a good pattern and polarization diversity, high gain with high efficiency, and wide matching bandwidth. In addition, a UWB broadside CP radiation characteristic can be achieved from the four elements by properly sequentially exciting the four ports simultaneously. We show that the design provides a compact MIMO antenna with a considerable size reduction because the radiating patch is the grounding plane of the microstrip line, exciting the next (neighbor) patch with orthogonal polarization in sequential order. The merged two antennas are thoroughly evaluated and then extended to a four-port MIMO design. All size-reduction properties and antenna characteristics are presented in Section II. This section is ended by comparing the un-merged and merged four-port designs and then describing the novel technique, step by step. In addition to the beam rotation feature of the linear polarization (LP) characteristics, a UWB CP performance of the four elements is achieved and discussed at the beginning of Section III. The semi-end-fire pattern in the LP mode is another interesting characteristic given in Section III. Using the surface current and E-field distributions on the structure, the isolation verification between the ports is performed for two resonant modes. At the end of Section III, the feed line positions are parametrically investigated. All related results are presented and compared. Finally, an off-center-fed sample is selected and introduced in addition to the first sample (i.e., the center-fed) to provide a wider matching and CP bandwidths. The MIMO performance is studied through the key parameters and proposed in Section IV. The measurements of the two prototypes are presented and compared with recently published results. Finally, the related discussions are presented in Section V. In Section VI, Conclusions, suggestions of some applications, and possible future works are presented.

## Step-by-Step Development of Sharing Technique

To reach a simple understanding of the proposed technique, a step-by-step procedure is presented. First, based on the frequency band of interest, a primary unit cell (i.e., a single antenna) should be designed as a subset of the final array. The proposed monopole based antenna is shown in Fig. 1(a) with two fundamental parameters, d, and g. The antenna is fabricated on a 1-mm FR4-based substrate ($\varepsilon_r$=4.4 and the loss tangent of 0.02). It is required to have symmetric shape and field distribution, of the objected four-port structure, in geometry and field distribution. Therefore, the radiating patch and its ground plane must be square and equal to each other, as illustrated in Fig. 1(a). It is expected that the port connectors will interact with the structure. Therefore, the SMA connectors effects are considered in all simulations to be close to the practical case, but still, the coaxial cables might have some effect, but not considered. Thus, it is possible to observe some differences between measured and computed results. Also, in this work, 3D E-field and 2D surface current distributions are studied to illustrate and verify the proposed technique. Hence, a suitable finite-element-based mesh based on the shortest wavelength is formed on the whole structure.

In order to cover a frequency band from 2 to 6GHz, d, and g in Fig. 1(a) are optimized and chosen to be 23.2 and 2.6 mm, respectively. As the radiating patch and ground plane are equal to each other, the structure in Fig. 1(a) is equivalent to an edge fed dipole (EFD), but the active excitation is located between the two patches. If the port is allocated between the patches, as

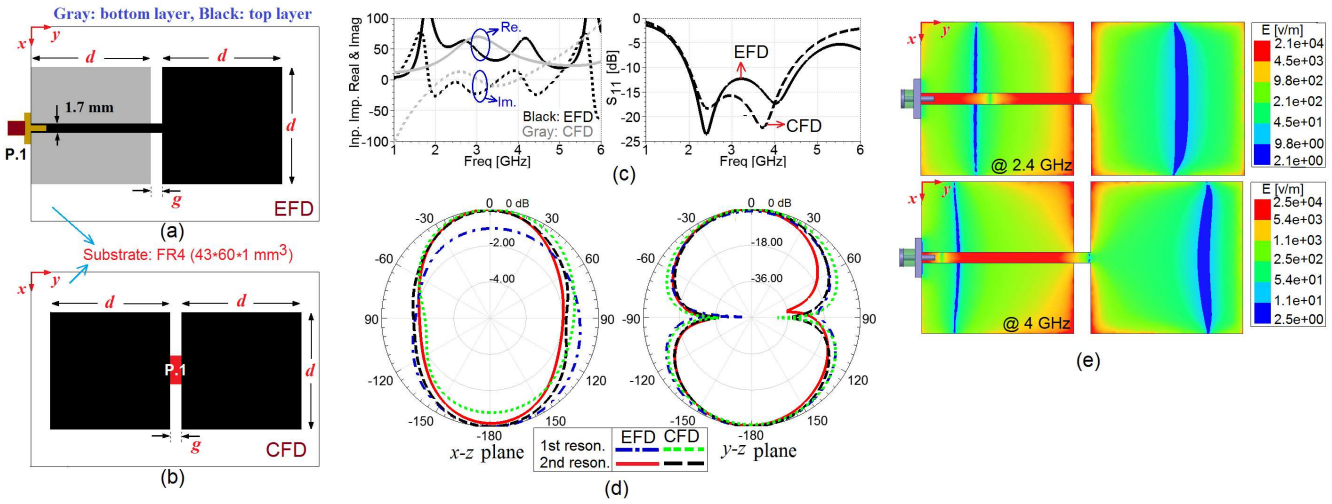


**Figure 1.** (a) Configuration of the proposed EFD, (b) configuration of the CFD, (c) input-impedance real and imaginary values and $S_{11}$, (d) x-z and y-z planes radiation patterns for EFD and CFD at the resonant frequencies, and (e) E-field distributions on EFD at both resonances.

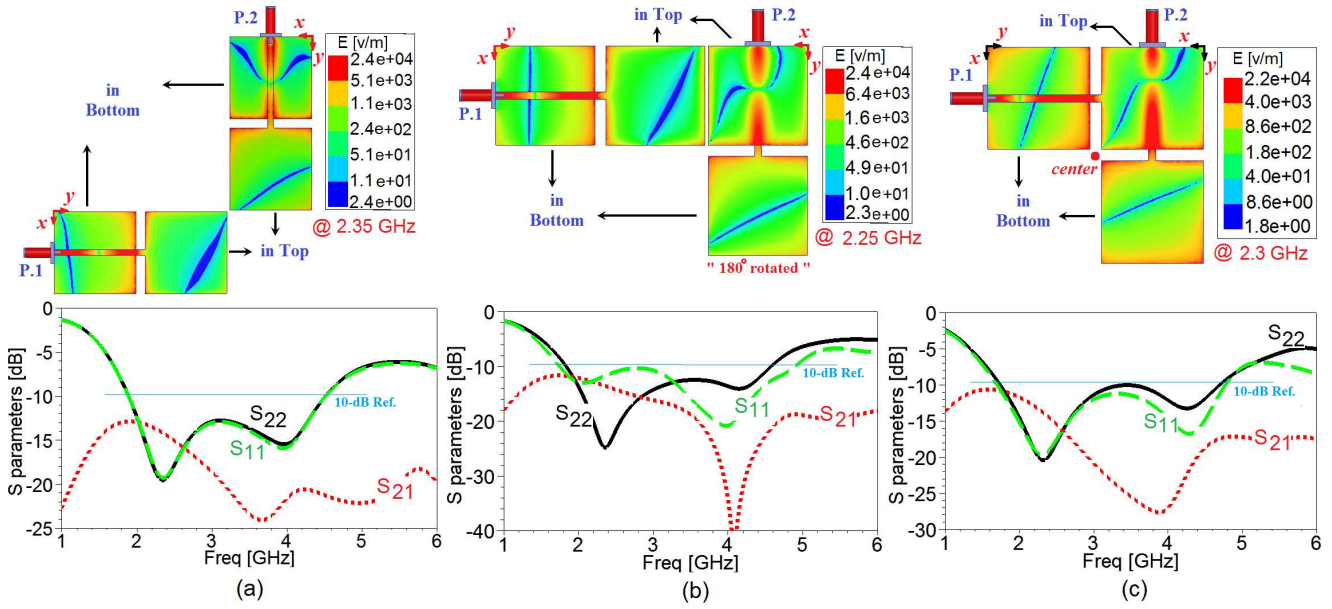


**Figure 2.** Extending process of a two-element array and final merging including the E-field distributions (when both ports are excited) and S parameters, (a) two antennas perpendicular to each other and far from each other, (b) two antennas side by side and perpendicular to each other (where Ant. 2 has been rotated 180 degrees relative to itself to make the ground plane of Ant. 2 level with the radiation patch of Ant. 1), and (c) a merged structure (where the radiation patch of Ant. 1 has been merged with the ground plane of Ant. 2, both in the top surface of the substrate).

illustrated in Fig. 1(b), a center-fed dipole (CFD) is clearly seen. In Fig. 1(c), S11 of the EFD and CFD show similar behavior with 10-dB bandwidth of 81.8% (1.95 4.65GHz). However, the input impedance differs due to the effect of the port location. Moreover, CFD shows that two resonance frequencies where the imaginary part about to changes from negative to positive or when it has a positive slope at (2.4 and 4 GHz). The radiation patterns of the EFD and CFD are similar, as shown in Fig. 1(d) except the little asymmetry in the H-plane of the edge fed case.

One could predict the effective quarter wavelength by the length between the left or the right edge of the patch to the position of the field null. So, roughly, at 2.4GHz, the total length is a little larger than one effective wavelength. At 4.0GHz, the total length is close to one and a half effective wavelength. Fig. 1(e) also shows the required uniform and symmetric E-field distribution close to the radiating and ground patches of the proposed antenna at both resonances.

In order to reach the main objective of having a 2×2 four-port structure, the two antennas in every pair are orthogonal, which enables the polarization orthogonality of the antennas to be used for enhancing the isolation. Hence, in the following, a

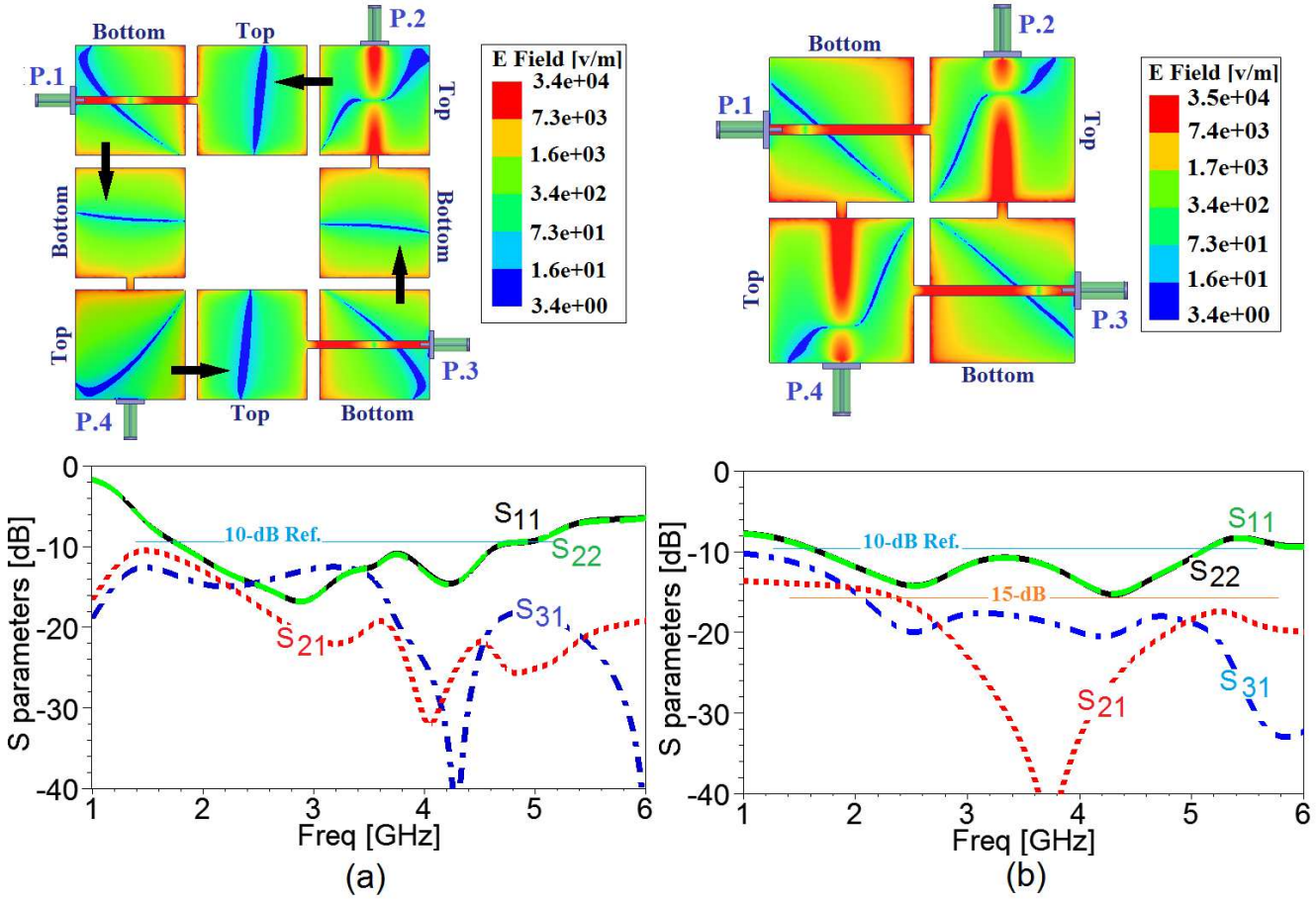


**Figure 3.** Two four-port antennas, their S parameters and E-field distributions (@ 2.5GHz, i.e., the fundamental resonance mode at both antennas) when all ports are excited, (a) the extended version of the two-element structure (un-merged design), proposed in Fig. 2(b), and (b) the proposed four-element square monopole array antenna (the first proposed prototype: the merged design) including the extended version of the two-element structure, shown in Fig. 2(c).

similar antenna is placed perpendicular to the first antenna (shown in Fig. 2(a)), which provides symmetry structure around the 45-degree plane of symmetry between them. In the presented field distribution in Fig. 2(a) (in which both ports are excited), a relative similarity is observed. This design occupies an ample space ($\equiv 3d\times3d$). Now, shift Ant 1 up to be aligned with the ground plane of Ant 2 and flip Ant 2 around itself, as shown in Fig. 2(b). The symmetry is lost, but the size is reduced.

The S-parameters lose the symmetry as clear from $S_{11}$ and $S_{22}$, but with little changes compared to those in Fig. 2(a). Now, shifting Ant 1 to the right to have its radiating patch overlap with the ground plane of Ant 2, a more compact structure is obtained, as shown in Fig. 2(c). By simultaneously exciting the two ports by equal signals, the field distribution indicates that the ground plane of Ant 1 has about the same field distribution as the radiating patch of Ant 2. The structure acts as it is close to being symmetry as the S-parameters are close to those in Fig. 1(c). Also, the structure acts as two dipoles with the right half of Ant 1 is overlapped with the top half of Ant 2.

At first glance, it is obvious that the occupied area by the new combination ($\simeq 2d\times2d$) is reduced 33% in comparison to the previous structure ($\simeq 2d\times3d$). Comparing the field distribution of these two structures, there is about an 8% reduction (from 2.4 to 2.2v/m) in the magnitude of the maximum field. Although the diagrams of the gain and efficiency are not presented here for brevity, their graphs, in comparison with those of the un-merged structure, demonstrate that this merging does not deteriorate the results. Moreover, the S-parameters have also remained almost unchanged compared to the results in Figs. 2(a) and (b).

The field distribution in Fig. 2(c) is about the same on the patches and the ground plane, which is symmetrical about the marked center point. The areas of the minimum field are all almost in the same directions, which are crossing the center point radially. This phenomenon demonstrates that such a combination can be copied and rotated about the mentioned center point to expand the array from two ports to four ports. To characterize the final structure based on the duplication and rotation, two examples of un-merged and merged four-port structures are presented in Figs. 3(a) and (b), respectively, for comparison. In an un-merged structure, a considerable field symmetry about the center of the structure is observed. For instance, there is a similarity between the minimum field on the ground plane of the second antenna and on the radiating patch of the first antenna,

TABLE 1
COMPARISON OF THE THREE DIFFERENT CHANNEL MEASUREMENT TECHNIQUES.

| Design: | Un-Merged | | | Merged | | |
|---|---|---|---|---|---|---|
| Frequency (GHz) | 2.5 | 3.4 | 4.3 | 2.5 | 3.4 | 4.3 |
| Gain [dBi] | 2.3 | 4.18 | 4.11 | 1.7 | 3.56 | 4.2 |
| Efficiency (%) | 90 | 83 | 87 | 92 | 82 | 88 |
| Total physical size | $74.8\times74.8\ mm^2$ | | | $49\times49\ mm^2$ | | |
| Bandwidth (%) | 97 | | | 101 | | |
| ($f_L$-$f_u$) GHz | (1.75-5.05) | | | (1.7-5.15) | | |
| min $\lvert S_{21}\rvert$ dB | 11 | | | 15 | | |
| min $\lvert S_{31}\rvert$ dB | 13 | | | 14.6 | | |

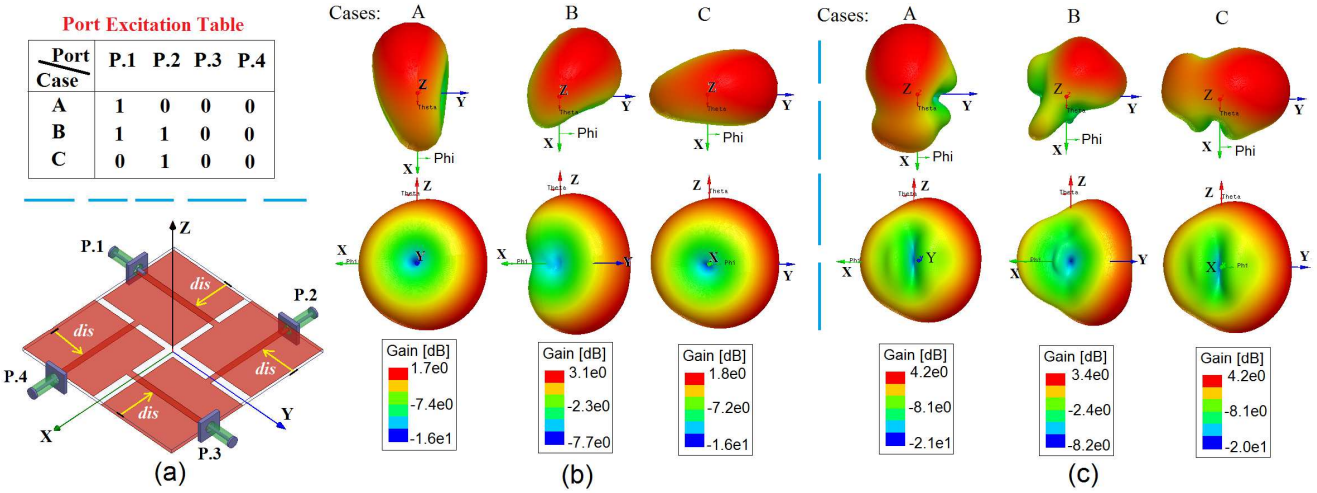


**Figure 4.** (a) Configuration of the proposed merged four-element array antenna (dis = 10.75mm) and the ports excitation table (for example in Case B, both P.1 and P.2 are excited, and the other ones are matched), (b) top (x-y plane) and side (x-z and/or y-z planes) views of the 3D radiation patterns at the first resonance (i.e., 2.5GHz), and (c) top (x-y plane) and side (x-z and/or y-z planes) views of the 3D radiation patterns at the second resonance (i.e., 4.3GHz).

and this similarity is repeated anticlockwise between the antenna pairs, i.e. 1 with 4, 4 with 3, and 3 with 2. Therefore, the ground planes are merged with the radiating patches in the direction of the presented black arrows (see Fig. 3(a)), and the final merged structure is achieved, as illustrated in Fig. 3(b). The field symmetry about the center of the structure is clear. Naturally, this phenomenon results in the enhancement of the symmetry of the radiation characteristics. Comparing the occupied area of the merged design ($\simeq$2d$\times$2d) with that of the un-merged structure ($\simeq$3d$\times$3d) demonstrates a 55.5% reduction in the size, which is considered as one of the important contributions of the proposed technique. Another outstanding characteristic of the merged design is the distance reduction between the radiating patches to 27mm, $0.23\lambda_0$ instead of $0.5\lambda_0$ in the conventional arrays at 2.6GHz.

A comparison between the S-parameters in Fig. 3 shows that $S_{11}$ (or $S_{22}$) frequency response has become more uniform by merging the antennas. The other radiation and impedance properties of these two designs are summarized in Table 1 indicate that the proposed merging increases the efficiency and bandwidth and isolation between ports. Besides, the total physical size of the merged design is reduced by 57%. One of the main reasons for the wideband performance is that each pair of patches acts as a dipole antenna with the port located at the dipole edge, where the current is always minimum regards of the dipole length. Therefore, the input impedance is not significantly varying.

## Beam Steering Capability, CP Radiation features, Isolation Verification and Parametric Study

For a MIMO system, especially in the new wireless system generations, the ability to rotate the radiation beam in azimuth (from phi = 0° to 360°) and cover different independent spaces by exciting specific ports can be beneficial. If we want to introduce the proposed design as a MIMO structure, the beam steering and rotation capability should be studied. It is noted that to specify the direction and shape of the beams, 3D radiation patterns have been selected in these studies. To cover specific directions,

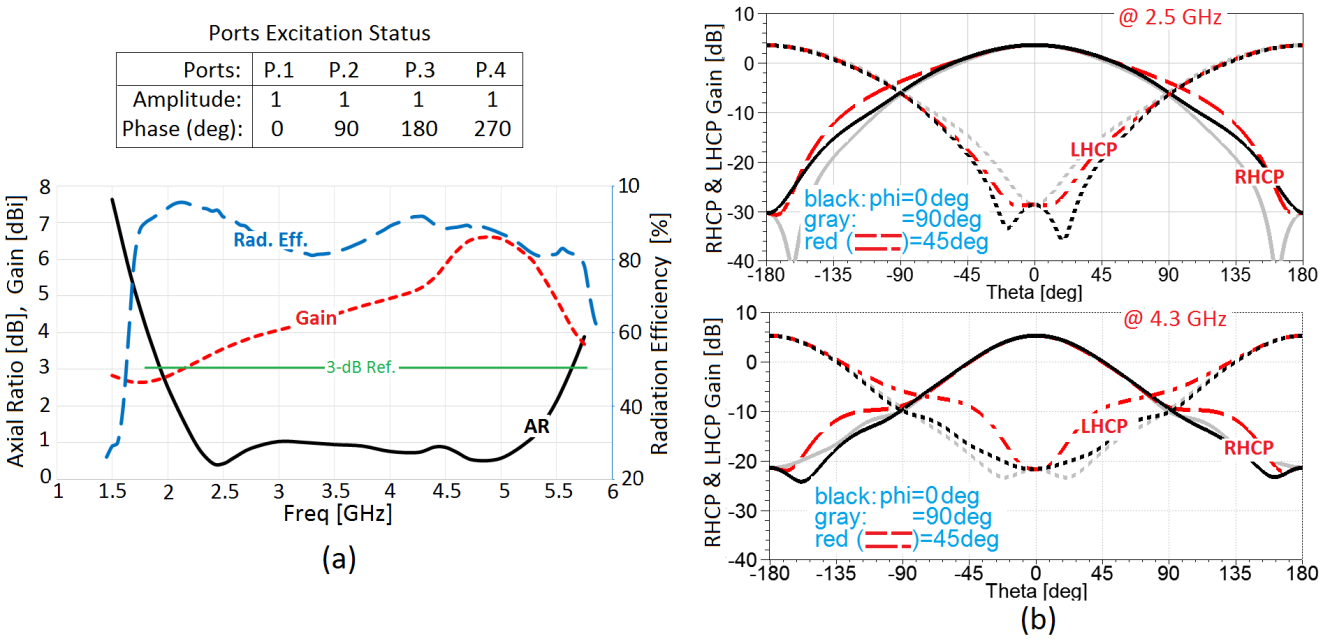


**Figure 5.** CP graphs of the first prototype (dis = 10.75mm) including (a) Ports excitation status and AR, Gain and Radiation Efficiency graphs, and (b) RHCP and LHCP graphs versus Theta for different Phi cuts (i.e., 0°, 45°, and 90°) at 2.5 and 4.3GHz.

the excitation statuses of the ports are presented in a table, shown in Fig. 4(a). The 3D radiation patterns are illustrated in Figs. 4(b) and (c) at two resonant frequencies, 2.5 and 4.3GHz, respectively. The 3D graphs on top of Figs. 4(b) and (c) prove that the radiation beam is rotated in clockwise mode by carefully selecting the excited ports, which occurs at both frequencies. Therefore, acceptable space diversity is provided. Based on these 3D radiation patterns, and unlike the broadside pattern expected for the proposed monopole-based antenna, it is interesting to observe that this design can direct the radiation in one direction. Minimum F/B of about 11dB, SLL lower than -12dB, and 3-dB beamwidth narrower than 60° are provided. Therefore, the produced pattern can be named as quasi-end-fire. It should be noted that this pattern is formed by exciting only one antenna (not an array with the capability of increasing the directivity) and so a very narrow beam-width cannot be expected. This phenomenon is a distinctive feature of the proposed design.

By feeding all ports in phase, only linear polarizations are obtained. Phase excitation can also be used to introduce more radiation states of different radiation directions as well as different polarizations, adding further MIMO capabilities. For example, if two pairs of ports exciting orthogonal patches are excited simultaneously with the same magnitude and 90-degree phase difference between them, a right hand (RH) or left hand (LH) circularly polarized (CP) radiation characteristics can be achieved depending on the phase between the two ports for a particular direction of the beam. The same phase differences between the ports will provide RHCP in one direction and LHCP in the opposite direction and vice versa. We believe that these characteristics are clear, and there is no need to present them for brevity. Here, we are only going to show the CP characteristics to produce a single broadside beam by exciting all four ports simultaneously with a sequence of 90-degree phase differences. The state of the excitation of all ports, axial ratio (AR), gain, and radiation efficiency graphs from 1 to 6GHz are presented in Fig. 5(a). The CP performance with high purity (AR < 1dB) from 2.2 to 5.25GHz, gain more than 3dBic with a maximum of 6.5dBic and efficiency higher than 81% over the entire band can be observed. Moreover, the 3-dB AR bandwidth is about 100% from 1.9 to 5.7GHz. It should be stated that by ideally controlling the phase and amplitude to all ports, the CP characteristics would have a wideband, but the matching of the antenna will limit such bandwidth. Also, if a feeding network is used to provide the required phase and amplitude distribution, the CP bandwidth will be significantly reduced.

As shown in Fig. 5(b), there is a significant difference (high purity) between RHCP and LHCP components, i.e., more than 30 and 25dB at 2.5 and 4.3GHz, respectively. This purity is available in both views, phi = 0° and 90°. Although, the cross-polar component (i.e., LHCP level) is enhanced in 45°-phi cut, especially at 4.3GHz, and so the purity is degraded as expected for the sequential feeding of linearly polarized elements. This can be improved if the elements are circularly polarized.

According to the merging applied to the proposed design between the radiation surfaces and the ground planes, the volume E-field distribution inside the substrate and the surface current distribution on all surfaces are used simultaneously to evaluate the isolation between some selected ports, ports 1 and 2 and ports 1 and 3. These distributions at 2.5 and 4.3GHz are illustrated in Figs. 6(a) and (b), respectively. Both types of distributions show that when the first port (P.1) is excited, only the surfaces

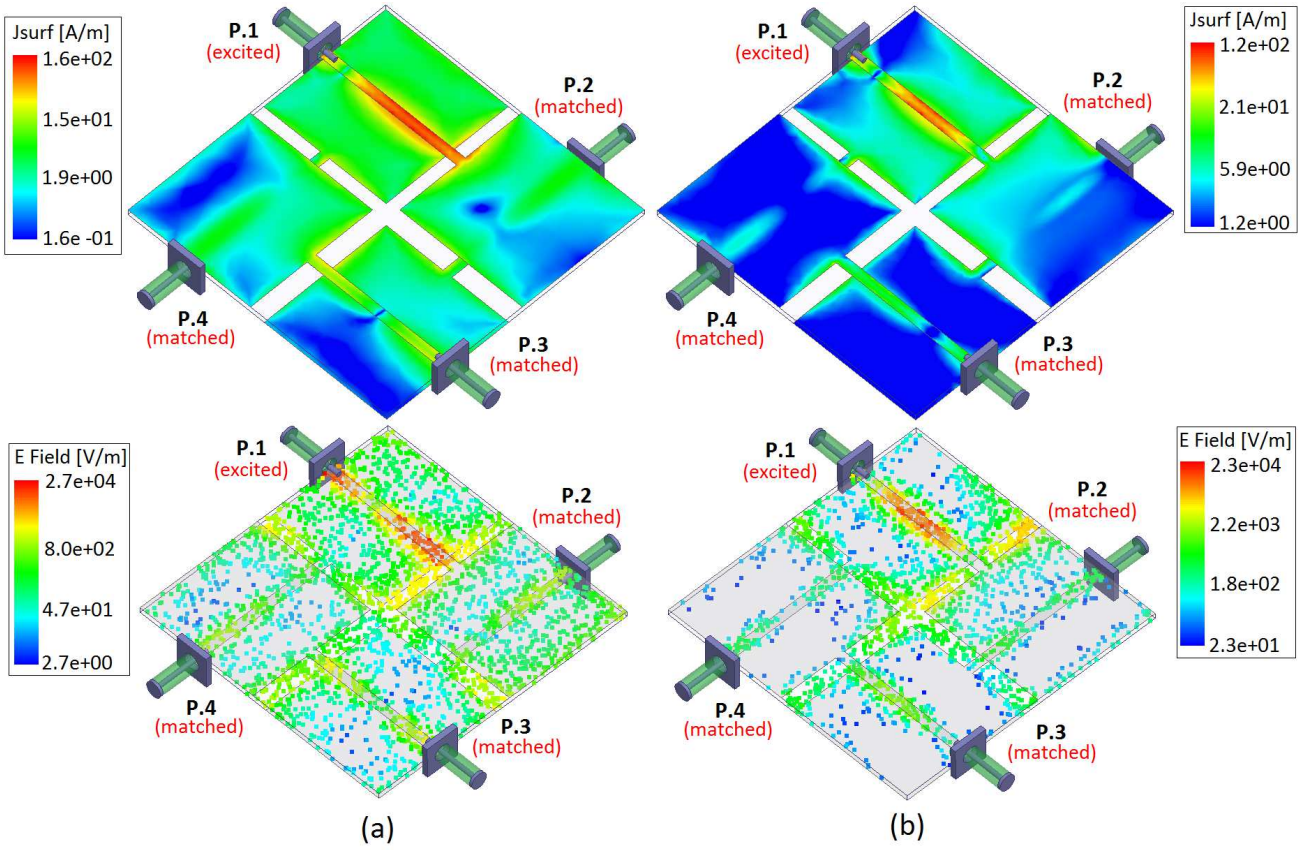


**Figure 6.** Surface current distribution on the conductor surfaces (top images) and 3D E-field distribution inside the substrate (bottom images) in the first prototype at (a) 2.5GHz, and (b) 4.3GHz.

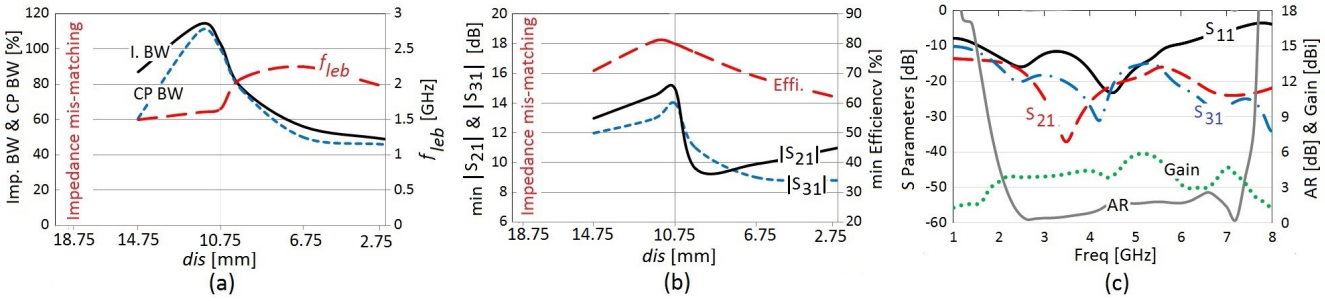


**Figure 7.** Study of the four-element MIMO antenna (shown in Fig. 4(a)), (a) 10-dB $S_{11}$ impedance and 3-dB AR bandwidths and the frequency of the Lower Edge of the covered Band (fleb) versus dis, (b) minimum values of $|S_{21}|$, $|S_{31}|$, and radiation efficiency versus *dis*, (c) impedance (S parameters), and radiation (gain and AR) graphs of the second prototype with dis = 11.75mm versus frequency.

and the quadrant of the substrate in front of that port has the highest amplitude of the current and the field, respectively. This indicates high isolation between the first port and the other ports. In addition, comparing the distributions at two resonances demonstrates that the isolations are stronger at the second resonance (4.3GHz). In the conventional printed monopole antennas, the ground plane has a single independent role, and its surface current is controlled only by its own connected port. On the contrary, in the presented method, this ground plane (e.g., the ground plane of the first antenna in Fig. 4(a)) also plays another role as a radiating patch of the other antenna (e.g., the fourth antenna in Fig. 4(a)), and its surface current is also adjusted by the port of that antenna (i.e., P.4). Therefore, changing the dis parameter (in Fig. 4(a)) causes the feed line of the first antenna to have different magnitudes of the current (excited by P.4) on its ground plane and so its impedance is changed, which results in variations in the impedance and radiation parameters of the presented structure. The results of these effects are illustrated in Figs. 7(a) and (b). According to Fig. 7(a), when dis is around 11.75mm, the maximum impedance and CP bandwidths are provided over 100%.

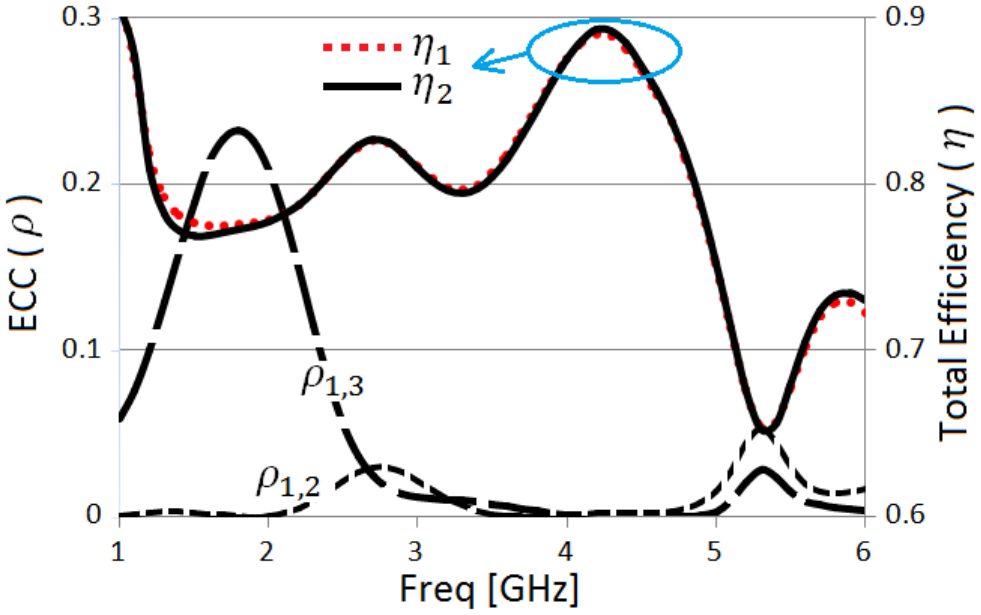


**Figure 8.** Calculated ECC (or $\rho_{i,j}$) and total efficiencies ($\eta_i$) of the first prototype ($dis$ = 10.75mm), where i=1.2 and j=2.3.

In addition, the minimum values for the lower end of the frequency band (i.e., fleb in Fig. 7(a)) belong to a region between dis = 11 and 14.75mm. The stronger isolations of $S_{21}$ and $S_{31}$, over 15.5 and 14.5dB, respectively, can be seen in a region between dis = 11 and 12mm, as shown in Fig. 7(b). This figure also demonstrates that the maximum efficiency is related to the mentioned region. According to these parametric studies, a second prototype (off-center-fed sample) is also selected in addition to the first one for enhancement of the performance. In the second design, dis is 11.75mm. The simulated S-parameters, gain, and AR of this prototype are presented in Fig. 7(c). It is found that the second sample of the proposed design with a 1 mm offset feeding-line has a relatively wider matching and 3dB-AR bandwidths in comparison to the first prototype with a central feed. This off-center-fed design proposes about 111% (2.1 7.3GHz) band-width of 3dB-AR and antenna gain higher than 3dBi with a maximum of 5.95dBi. Besides, the impedance bandwidth is 109% (1.7 5.75GHz), with the isolations better than 15dB.

## MIMO Performance Evaluation

In order to have a good MIMO performance from the proposed design of four merged antennas, some key parameters including the ECC, diversity gain (DG), total efficiency, and MEG must be determined to be sure that they are within the standard range. The ECC is a measure of the MIMO radiation diversity, which can be calculated by both the radiation fields and the S-parameters. However, the S-parameters approach is not valid for lossy structure[31]. Therefore, it is more accurate to calculate ECC (or $\rho_e$) from the far-field radiation patterns as given[8,9,33]:

$$\rho_e = \frac{|\iint_{4\Pi} F_1(\theta\cdot\varphi)^* \bullet F_2(\theta\cdot\varphi))d\Omega|^2}{\iint_{4\Pi}|F_1(\theta\cdot\varphi)|^2 d\Omega \times \iint_{4\Pi}|F_2(\theta\cdot\varphi)|^2} \tag{1}$$

where $F_i$ $(\theta.\phi)$ is the radiation field of the ith antenna, $\Omega$ is the solid angle, and "•" denotes the Hermitian product. It is noted that in the calculation and measurement of the far-field pattern (presented in the next section), the uniform outdoor propagation environment is assumed, and the cross-polarization discriminator (XPR) is equal to 1.

We know from[6] that a lower ECC leads to a higher capacity and an enhanced diversity gain. As shown in Fig. 8, the correlation graphs ($\rho_1.2$ and $\rho_1.3$) of the first prototype propose a low ECC less than 0.22 in the whole band. In the second prototype, these parameters have a maximum ECC of 0.23, which is not presented in this section for brevity. The obtained maximum ECCs satisfy the criteria of low correlation ($\rho_e < 0.5$) of MIMO. Thus, good diversity performance is expected.

Another parameter DG is the amount of progress obtained from an array system relative to a single antenna. This parameter is calculated by:

$$DG = 10\sqrt{1-|ECC|^2} \tag{2}$$

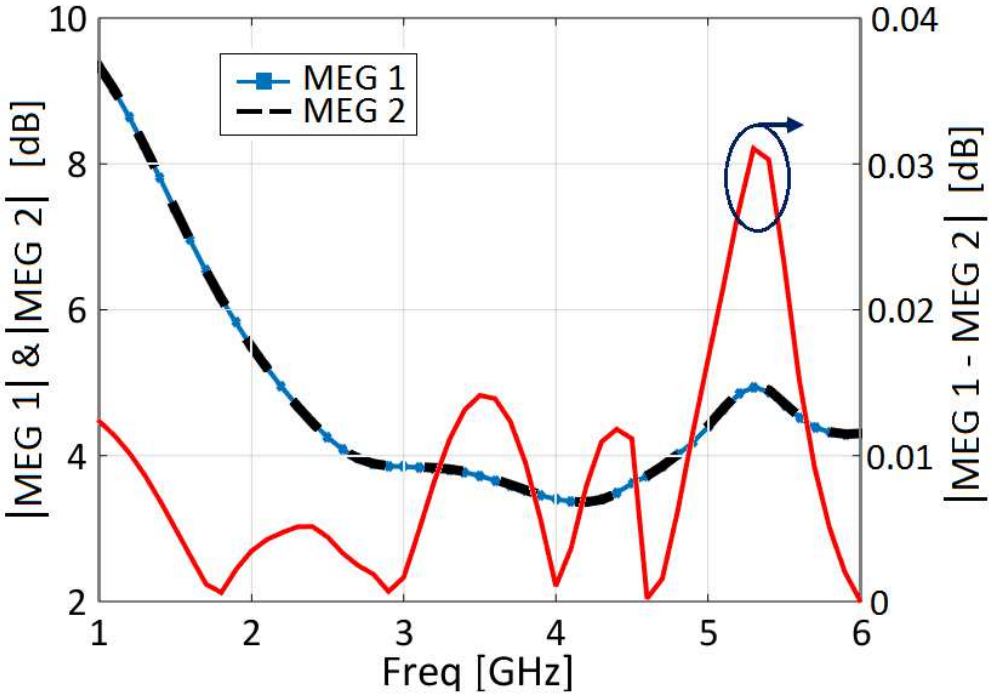


**Figure 9.** Calculated $MEG_i$ ($i$=1. 2 ) and $MEG$ difference.

By using the above mentioned maximum ECCs in (2), the minimum values of DGs are calculated in the whole band, which are equal to 9.75 and 9.73, respectively. These results guarantee good MIMO performance. The other parameter is total efficiency, which is calculated by (3)[20,33] for the ith antenna.

$$\eta_{Total.\ i} = \left(1 - |S_{ii}|^2 - \sum_{j \neq i} |S_{ij}|^2\right) \times \eta_{Radiation.\ i} \tag{3}$$

where, $\eta_{(Radiation.i)}$ is the radiation efficiency of the ith antenna with the other antennas terminated by matched loads. As illustrated in Fig. 8, $\eta_1$ and $\eta_2$ propose the minimum and maximum efficiencies of about 0.775 (i.e., 77.5%) around 1.8GHz and 0.89 (i.e., 89%) around 4.2GHz, respectively. Due to the lossy substrate, these efficiencies are quite significant. In the second prototype, the minimum and maximum efficiencies are about 81% and 85%, respectively.

The final parameters are the MEG and MEGs difference. The MEG parameter is the ratio of the mean received power of the antenna to total mean incident power at the antenna[8] which is calculated by:

$$MEG = \oint \left[\frac{XPR}{1+XPR} P_\theta(\Omega) G_\theta(\Omega) + \frac{1}{1+XPR} P_\varphi(\Omega) G_\varphi(\Omega)\right] d\Omega \tag{4}$$

where $G_\theta$ and $G_\phi$ are the $\theta$ and $\phi$ polarized components of the antenna gain pattern and $P_\theta$ and $P_\phi$ are the $\theta$ and $\phi$ components of the angular density functions of incoming plane waves. As mentioned above, the uniform propagation environment is assumed in the calculation and hence XPR=1 and $P_\theta$=$P_\phi$=$1/4\pi$.$MEG_1$, $MEG_2$ (both calculated by (4)) and their difference is shown in Fig. 9. This figure shows good MEG performance of the proposed design, as the difference between the MEGs is less than 0.1dB (i.e., the ratio is close to 1). In the second prototype, the difference between the MEGs is less than 0.3dB in the whole band.

## Fabrication, Measurement, Comparison and Discussion

In this section, both samples, center-fed, and off-center-fed designs have been implemented and measured. Their photos are shown in Figs. 10(a) and (b), respectively. In the measurement process, a four-port ZVA-67 vector network analyzer (VNA) (top image in Fig. 10(b)) is used. According to the physical symmetry between the four ports, only $S_{11}$, $S_{21}$, and $S_{31}$ have been measured. Bottom images in Fig. 10 show these measured S-parameters for both prototypes. In the center-fed sample, the

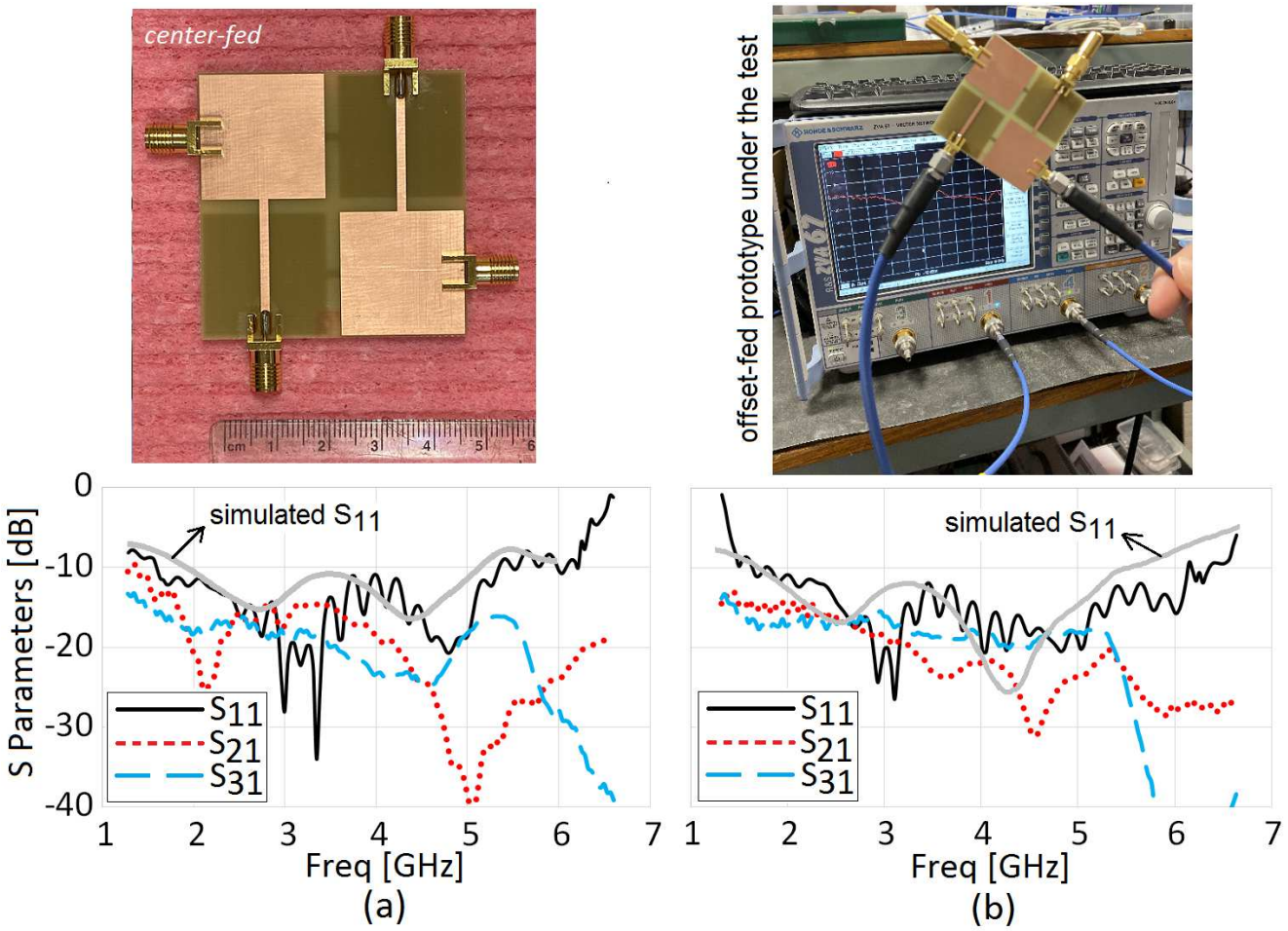


**Figure 10.** Photograph of the fabricated prototypes and their measured S parameters, (a) center-fed, and (b) off-center-fed.

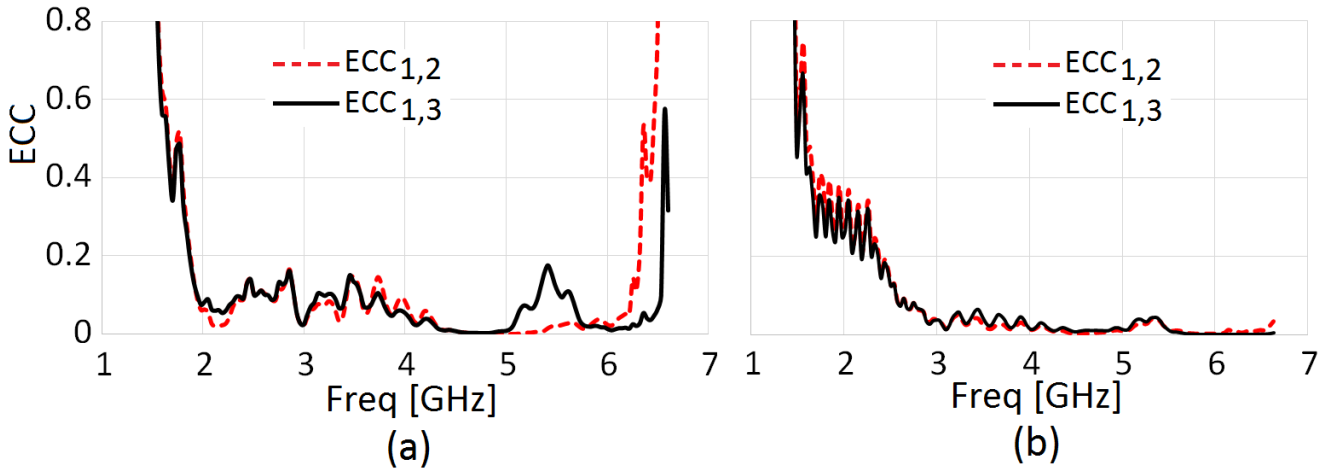


**Figure 11.** Measured $ECC_{1,2}$ and $ECC_{1,3}$, (a) center-fed, and (b) off-center-fed.

10dB-$S_{11}$ bandwidth is about 107.4% from 1.61 to 5.35GHz. The bandwidth for the second sample is about 115.7% from 1.63 to 6.11GHz. The matching ($S_{11}$) in both designs is good. In addition, an acceptable agreement between the simulated and measured $S_{11}$ graphs is observed. Minimum isolations for center-fed and off-center-fed proto-types are about 15 and 15.5dB, respectively. It must be noted that the amplitude ripple observed in the measured $S_{11}$ graphs has been occurred due to different

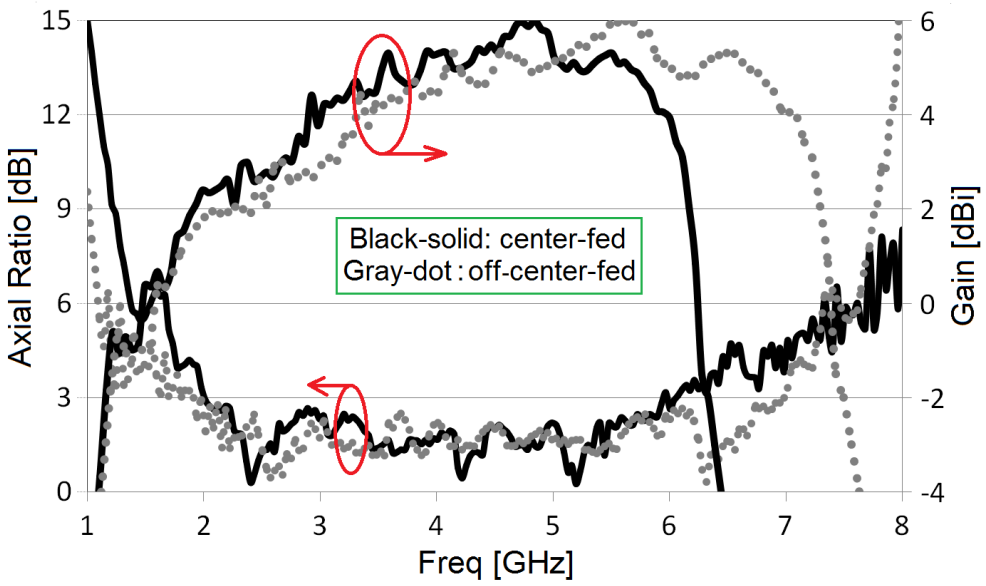


**Figure 12.** Measured AR and Gain for both center and off-center-fed prototypes.

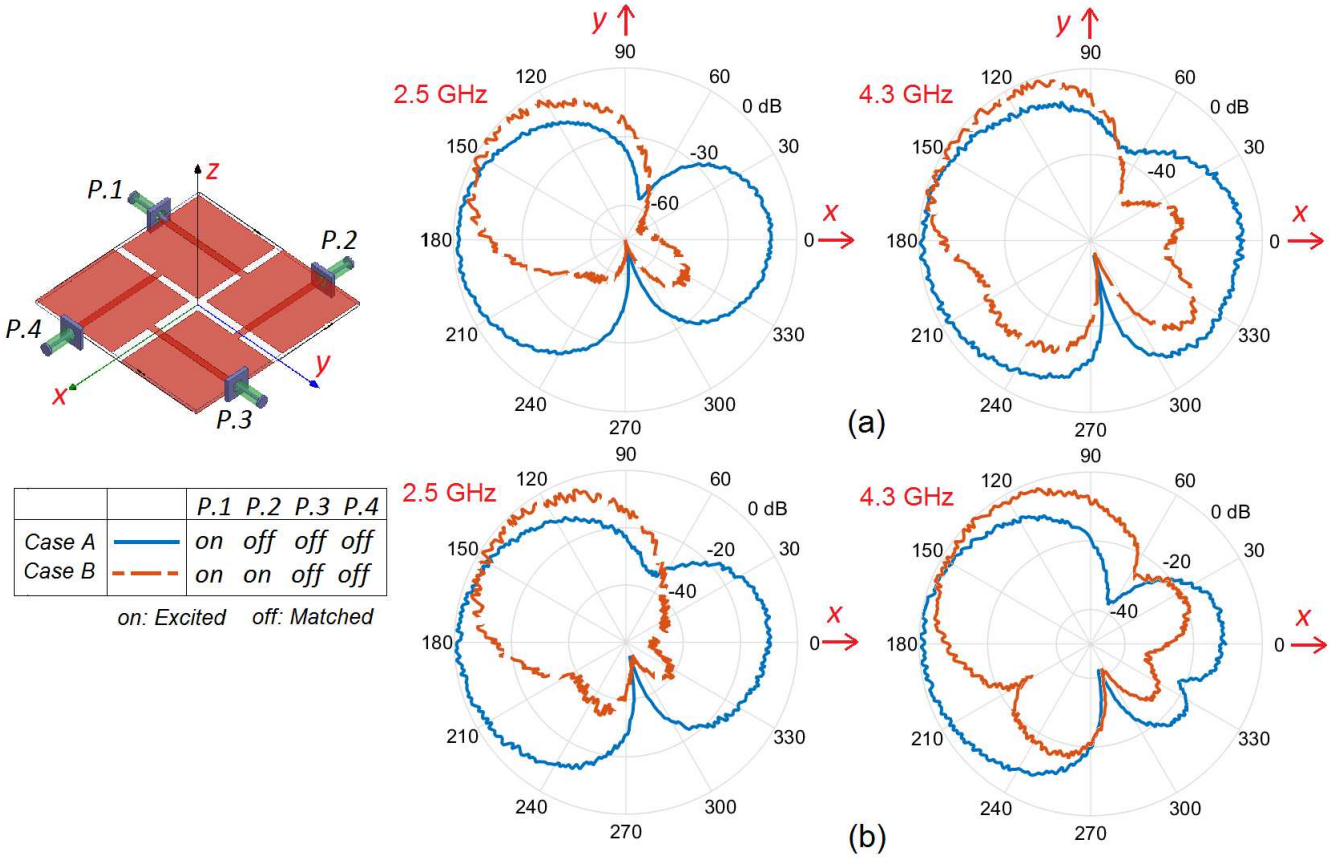


**Figure 13.** Measured x-y plane radiation patterns for two cases, A and B (see Fig. 4(a)), at 2.5 and 4.3 GHz: (a) center-fed, and (b) off-center-fed prototypes.

reasons such as the proximity of the DUT with the surrounding structures as well as the effect of the cables connecting the antenna to the VNA. $ECC_{1,2}$ and $ECC_{1,3}$ parameters are also measured, as presented in Figs. 11(a) and (b) for center-fed and

TABLE 2
COMPARISON OF THE THREE DIFFERENT CHANNEL MEASUREMENT TECHNIQUES.

| Works | Total size | Bandwidth | Isolation | Peak Gain | Peak Eff. | ECC | Complexity |
|---|---|---|---|---|---|---|---|
| [21] | 1.2λ0× 1.2λ0 (150 mm×150 mm) | (3.2%) 2.4∼2.48 GHz | >32 dB | 7.2 dBi | 81% | <0.05 | RH(with mush-room loads) |
| [22] | 0.33λ0× 0.33λ0 (45 mm×45 mm) | (96.2%) 2.2∼6.28 GHz | >14 dB | 4 dBi | 91% | <0.25 | Low |
| [23] | 0.45λ0× 0.27λ0 (42 mm×25 mm) | (115%) 3.2∼12 GHz | >21 dB | 4 dBi | 91% | <0.01 | Low |
| [24] | 0.36λ0× 0.36λ0 (40 mm×40 mm) | (58.6%) 2.7∼4.94 | >11 dB | 4.3 dBi | 95% | <0.1 | Low |
| [26] | 0.38λ0× 0.38λ0 (38.3 mm×38.3 mm) | 3∼5.2 & 6.2∼13.2 GHz | >17 dB | 5.8 dBi | 96% | <0.02 | Moderate |
| [27] | 0.39λ0× 0.39λ0 (40 mm×40 mm) | (130%) 2.94∼14 | >16 dB | 4.9 dBi | 88% | <0.04 | RH (with VIAs) |
| Present | 0.277λ0× 0.277λ0 (49 mm×49 mm) | (109%) 1.7∼5.75 | >15 dB | 5.9 dBi | 96% | <0.23 | Low |

off-center-fed prototypes, respectively. A maximum of about 0.35 in the whole band is detected for the ECC of both samples, which guarantees acceptable MIMO-diversity performance.

Fig. 12 shows the measured AR and gain parameters for both samples. It is noted that in AR measurement process, four ports of VNA (as can be seen in Fig. 10(b)) are employed simultaneously with equal signal amplitude and a sequence of 90° phase differences, and then connected to four ports of the prototype in the proper order. A broadband CP Helical antenna is used as a transmitter under the far-field distance condition (i.e., a distance of about 1.5 meters). In the center-fed prototype, 3dB-AR bandwidth is about 92% (2.1-5.8GHz) with maximum and minimum gains of about 6.1 and 2.2dBi, respectively. The off-center-fed prototype presents 3dB-AR bandwidth of about 111% (1.95-6.9GHz). The maximum and minimum gains are about 6dBi and 1.8dBi, respectively. In comparison to the simulated CP bandwidths, the measured ones are reduced by about 8% and 4% in center-fed and off-center-fed designs, respectively.

The radiation patterns at 2.5 and 4.3GHz, measured in an anechoic chamber, are presented in Figs. 13(a) and (b) for center-fed and off-center-fed prototypes, respectively. Due to the symmetry and for brevity, only two cases, A and B (i.e., A: P.1 is excited, and the others are matched, and B: both P.1 and P.2 are excited, and the other two ports are matched, as shown in the table in Fig. 4(a) and Fig. 13) are considered in the measurement for evaluating the main-beam rotation ability. As can be seen, in Case A, the main beam is along –x-axis (i.e., phi = 180º), and in Case B, the main beam is rotated about 45º and placed in phi = 135º direction. Moreover, these patterns indicate that the F/B ratio is more than 11dB in all cases. As a result, the proposed designs provide radiation directed in one direction with an almost end-fire shape and 360° beam rotation ability.

A comparison with details is presented in Table 2. Comparing to the other references reported in recent years, the proposed four-element MIMO structure is significantly small with a total area of $0.07\lambda_0^2$. In addition, at least 15dB isolation with a peak gain and efficiency of 5.9dBi and 95%, respectively, are obtained. In[23] and[27], a wider bandwidth is achieved, but lower gain and efficiency were presented. Moreover, the structure in[27] has some VIAs which increase the complexity of the design and fabrication. The multi-layer design in[21] has good gain and isolation, but it suffers from narrow bandwidth and mushroom-like loadings. Furthermore, the peak gain and efficiency of more than 5.8dBi, and 95% were provided in[26] with a dual-frequency-band behavior. Among these appropriate references, the low-complexity structure in[22] is a more acceptable four-port MIMO design with a small size and high bandwidth and efficiency.

## Conclusion

A novel design of a compact four-element array antenna suitable for wireless technologies such as 4G, 5G, and B5G has been presented. The design has passed through several steps to provide some understanding. In order to allow for having the radiating patch to be a ground plane of another patch, the size of the patch and the ground plane must be equal in size and shape, and the proper shape has to be square. Each orthogonal pair of this antenna can be merged to provide a more compact structure. It has been demonstrated that the primary merged structure could be extended from two ports to more than two ports as there was a specific field symmetry. In comparison to recently published works, the proposed array design has a significant size reduction over 50%, preserving the radiation efficiency and the bandwidth.

The other outstanding characteristic of the work was its unexpected semi-end-fire radiation with a minimum F/B ratio of

11dB, whose orientation was changed over 360° in azimuth by exciting the ports, one by one. In the following, it was shown that the wideband broadside CP performance could also be obtained by exciting all ports with 90º phase differences. Normally, CP bandwidth over 100% cannot be achieved through four conventional orthogonal monopole antennas, while this capability was obtained in the proposed design. The proposed antenna has a minimum isolation of 15dB between all ports and high peak gain and efficiency stable in the whole band. In addition, the appropriate values of the MIMO key parameters, especially ECC less than 0.23 and very good MEG and DG, show a proper MIMO diversity behavior for the merged design. Based on the achieved characteristics, the presented design can be very promising for future compact array designs with a high number of antennas in a limited space and with various wideband polarization characteristics.

## References


1. Zh. Zhang, Y. Xiao, Zh. Ma, M. Xiao, Zh. Ding, X. Lei, G. K. Karagiannidis, and P. Fan, "6G Wireless Networks: Vision, Requirements, Architecture, and Key Technologies," IEEE Vehicular Tech. Mag.,vol. 14, no. 3, pp. 28-41, Sep. 2019.
2. J. G. Andrews, S. Buzzi, W. Choi, S. V. Hanly, A. Lozano, A. C. K. Soong, and J. Ch. Zhang, "What Will 5G Be?" IEEE Jour. on Selected areas in Com., vol. 32, no. 6, pp. 1065-1082, June 2014.
3. Th. S. Rappaport, Sh. Sun, R. Mayzus, H. Zhao, Y. Azar,K. Wang, G. N. Wong, J. K. Schulz, M. Samimi, and F. Gutierrez, "Millimeter Wave Mobile Communications for 5G Cellular: It Will Work!" IEEE Access, vol. 1, pp. 335 – 349, 2013.
4. E. G. Larsson, O. Edfors and F. Tufvesson, and Th. L. Marzetta, "Massive MIMO for Next Generation Wireless Systems," IEEE Communications Mag., vol. 52, no. 2, pp. 186-195, Feb. 2014.
5. H. Xu, S. Gao, H. Zhou, H. Wang, and Y. Cheng, "A Highly Integrated MIMO Antenna Unit: Differential/Common Mode Design," IEEE Trans. on Antennas and Propag., Early Access, DOI: 10.1109/TAP.2019.2922763.
6. L. Zhao, L. K. Yeung, and K. -L. Wu, "A Coupled Resonator Decoupling Network for Two-Element Compact Antenna Arrays in Mobile Terminals," IEEE Trans. on Antennas and Propag., vol. 62, no. 5, pp. 2767-2776, May 2014.
7. K. –L. Wu, C. Wei, X. Mei, and Z. Y. Zhang, "Array-antenna Decoupling Surface," IEEE Trans. on Antennas and Propag., vol. 65, no. 12, pp. 6728-6738, Dec. 2017.
8. M. S. Sharawi, "Printed Multi-Band MIMO Antenna Systems and Their Performance Metrics," IEEE Antennas and Propag. Mag., vol. 55, no. 5, pp. 218-232, Oct. 2013.
9. R. Zaker, "Design of a Very Closely-spaced Antenna Array with a High Reduction of Mutual Coupling Using Novel Parasitic L-shaped Strips," Int. Jour. RF and Microw. Computer-Aided Eng., vol. 28, no. 9, May 2018.
10. Ch. F. Ding, X. Y. Zhang, Ch. D. Xue, and Ch. –Y. -D. Sim, "Novel Pattern-Diversity-Based Decoupling Method and Its Application to Multi-element MIMO Antenna," IEEE Trans. on Antennas and Propag., vol. 66, no. 10, pp. 4976-4985, Oct. 2018.
11. Y. –F. Cheng and K. –K.-M. Cheng, "A Novel Dual-Band Decoupling and Matching Technique for Asymmetric Antenna Arrays," IEEE Trans. on Microw. Theory and Tech., vol. 66, no. 5, pp. 2080-2089, May 2018.
12. Ch. –H. Wu, Ch. –L. Chiu, and T. –Gh. Ma, "Very Compact Fully Lumped Decoupling Network for a Coupled Two-element Array," IEEE Ant. and Wire. Propag. Lett., vol. 15, pp. 158-161, 2016.
13. X. Zhao, S. P. Yeo and L. Ch. Ong, "Planar UWB MIMO Antenna with Pattern Diversity and Isolation Improvement for Mobile Platform Based on the Theory of Characteristic Modes," IEEE Trans. on Antennas and Propag., vol. 66, no. 1, pp.420-425, Jan. 2018.
14. X. Zhao, S. P. Yeo and L. Ch. Ong, "Decoupling of Inverted-F Antennas with High-Order Modes of Ground Plane for 5G Mobile MIMO Platform," IEEE Trans. on Antennas and Propag., vol. 66, no. 9, pp. 4485-4495, Sep. 2018.
15. K. Wei, J. –Y. Li, L. W., Z. Xing, R. Xu, "Mutual Coupling Reduction by Novel Fractal Defected Ground Structure Band-gap Filter," IEEE Trans. on Antennas and Propag., vol. 64, no. 10, pp. 4328-4335, Oct. 2016.
16. S. Gupta, Z. Briqech, A. R. Sebak, and T. A. Denidni, "Mutual-Coupling Reduction Using Metasurface Corrugations for 28 GHz MIMO Applications," IEEE Ant. and Wire. Propag. Lett., vol. 16, pp. 2763-2766, 2017.
17. Y. –F. Cheng,X. Ding,W. Shao, andB. –Zh. Wang, "Reduction of Mutual Coupling Between Patch Antennas Using a Polarization-Conversion Isolator," IEEE Ant. and Wire. Propag. Lett., vol. 16, pp. 1257-1260, 2017.
18. Zh. Zhao, A. Zhang, X. Chen, G. Peng, J. Li, H. Shi, and A. A. Kishk, "Mutual Coupling and Correlation of Closely Spaced Patch Antennas," Electronics Letters, vol. 55, no. 13, 2019.

**19.** M. Karaboikis, C. Soras, G. Tsachtsiris and V. Makios, "Four-element Printed Monopole Antenna Systems for Diversity and MTMO Terminal Devices," Inter. Conf. on Applied Electromag. and Comm., Croatia 2003.

**20.** Ch. –Y. Chiu and R. D. Murch, "Compact Four-Port Antenna Suitable for Portable MIMO Devices," IEEE Ant. and Wire. Propag. Lett., vol. 7, pp. 142-144, 2008.

**21.** G. Zhai, Zh. N. Chen, and X. Qing, "Mutual Coupling Reduction of a Closely Spaced Four-element MIMO Antenna System Using Discrete Mushrooms," IEEE Trans. on Microw. Theory and Tech., vol. 64, no. 10, pp. 3060-3067, Oct. 2016.

**22.** R. Anitha, P. V. Vinesh, K. C. Prakash, P. Mohanan, and K. Vasudevan, "A Compact Quad Element Slotted Ground Wideband Antenna for MIMO Applications," IEEE Trans. on Antennas and Propag., vol. 64, no. 10, pp. 4550-4553, Oct. 2016.

**23.** G. Srivastava, and A. Mohan, "Compact MIMO Slot Antenna for UWB Applications," IEEE Ant. and Wire. Propag. Lett., vol. 15, pp. 1057-1060, 2015.

**24.** D. Sarkar,and K. V. Srivastava, "A Compact Four Element MIMO/Diversity Antenna with Enhanced Bandwidth," IEEE Ant. and Wire. Propag. Lett., vol. 16, pp. 2469-2472, 2017.

**25.** N. –Sh. Nie, X. –S. Yang, and B. –Zh. Wang, "A Compact Four-element Multiple-Input-Multiple-Output Antenna with Enhanced Gain and Bandwidth," Microw. Opt. Technol. Lett., vol. 61, no. 7, pp. 1828-1834, July 2019.

**26.** R. G. Villanueva and H. J. Aguilar, "Compact UWB Uni-Planar Four Port MIMO Antenna Array with Rejecting Band," IEEE Ant. and Wire. Propag. Lett., Early Access, DOI: 10.1109/LAWP.2019.2942827.

**27.** A. A. R. Saad, and H. A. Mohamed, "Conceptual Design of a Compact Four-element UWB MIMO Slot Antenna Array," IET Microw., Anten. and Propag., vol. 13, no. 2, pp. 208-215, 2019.

**28.** A. -D. Capobianco, F. M. Pigozzo, A. Assalini, M. Midrio, S. Boscolo, and F. Sacchetto, "A Compact MIMO Array of Planar End-Fire Antennas for WLAN Applications," IEEE Trans. on Antennas and Propag., vol. 59, no. 9, pp. 3462-3465, Sep. 2011.

**29.** Y. Pan, Y. Cui, and R. Li, "Investigation of a Triple-Band Multibeam MIMO Antenna for Wireless Access Points," IEEE Trans. on Antennas and Propag., vol. 64, no. 4, pp. 1234-1241, Apr. 2016.

**30.** S. S. Jehangir, and M. S. Sharawi, "A Wideband Sectoral Quasi-Yagi MIMO Antenna System with Multibeam Elements," IEEE Trans. on Antennas and Propag., vol. 67, no. 3, pp. 1898-1903, Mar. 2019.

**31.** A. T. Abed and A. M. Jawa, "Compact Size MIMO Amer Fractal Slot Antenna for 3G, LTE (4G), WLAN, WiMAX, ISM and 5G Communications," IEEE Access, DOI: 10.1109/ACCESS.2019.2938802.

**32.** I. Messaoudene, S. Aidel, T. A. Denidni, and A. A. Kishk, "Quarter Cylindrical Dielectric Resonator Antenna with Circular Polarization for Wideband MIMO Systems," Electronics Letters, to be published.DOI: 10.1049/el.2019.3138.

**33.** M. S. Sharawi, "Current Misuses and Future Prospects for Printed Multiple-Input, Multiple-Output Antenna Systems," IEEE Antennas & Propag. Mag., vol. 59, no. 2, pp. 162-170, Apr. 2017.